A Methodology for Sensor Positioning Based on Eigenmode data

P.J. Antunes, R.J. Guimarães, N.J. Ferreira, J.C. Viana, G.R. Dias

Critical Materials S.A., SpinPark - Centro de Incubação Tecnológica,

Zona Industrial da Gandra, 4806-909 Guimarães, Portugal

Abstract: The importance of sensor location is crucial for a correct assessment of the dynamic response of structures and, if early structural damage detection is a concern, for increasing the POD-Probability of Detection of Structural Health Monitoring (SHM) vibration-based methods. Also, the high cost of sensoring equipment (accelerometers, strain-gauges, fibre-optic sensors, etc…) implies the use of a minimum number of sensors that must be judiciously positioned in order to extract adequate and relevant information from the monitored structure. Critical Materials S.A. is developing algorithms for sensor positioning procedures, as an auxiliary tool for the deployment of vibration-based SHM techniques, based on Eigenmode and Eigenfrequency data retrieved from natural frequency extraction analysis procedures. Abaqus FEA-Finite Element Analysis platform, due to its capability in terms of dynamic analysis procedures and API-Application Programming Interface, contributes to the effectiveness and executability of the proposed sensor positioning methodology. The developed algorithms are capable of positioning accelerometers and/or strain sensors in function of the evaluation metrics used for the study and the specifications of the user. Several case-studies are presented and the proposed methodology is experimentally evaluated for the positioning of accelerometers in orthotropic CFRP-Carbon Fibre Reinforced Polymer composite based structures.

1. Introduction

The importance of sensor locations is crucial for a correct assessment of the dynamic response of structures and damage detection. Also, the high cost of sensoring equipment implies the use of a minimum number of sensors that must be judiciously positioned in order to extract adequate information from the monitored structure.

There are three major engineering applications for sensor positioning procedures (Staszewski & Worden, 2001), namely:

1. System/modal identification;
2. Control engineering;
3. SHM and damage detection.

From the above three application areas, the SHM and damage detection was the one that received least attention from the researchers. In fact, the control of the system observability, and controllability based on methods such as MKE-Modal Kinetic Energy (Lia, et al., 2007) and EFI-Effective Independence Method (Meo & Zumpano, 2005) (Hanis & Hromick, 2012) and Fisher information (BASSEVILLE, et al., 1987) matrix and EVP-Eigenvalue Vector Product (Meo & Zumpano, 2005) guarantees a more correct distribution of sensors based on the modal identification parameters. However, these techniques cannot guarantee an optimized positioning for damage detection that can be applicable in SHM systems.

In recent years, with the continuously growing importance of SHM techniques, sensor positioning methods gained more relevance in SHM related technical literature. Normally, these methods rely on numerical models (FE or analytical) to simulate damage in several location of the component and to enhance the sensitivity of sensoring equipment to a multiple cases of possible damaged spots within the considered structure.

In (Worden & Burrows, 2001), the combination of combinatorial optimization methods, such as genetic algorithm and simulated annealing was used to optimize sensor placement for fault detection using a model-based approach. Damage was induced at the FE level by removing small group of elements from the model (equivalent to setting the material's Young modulus to zero). Optimized sensor distributions were analysed and ordered in function of the probability of correct classification of damage. Also in (Beal, et al., 2008), a method of sensor positioning is presented for enhancing the sensitivity to structural stiffness changes. The method was applied in a 10-DOF system and the damage is induced via affection of the spring's stiffness. Aggregate relative changes in transfer functions, for damaged and baseline structures were used for defining the objective function. The inverse problem is solved numerically using a generalized mixed variable pattern search algorithm. In (Manson & Worden, 2001), a rectangular plate model was used as a case-study to optimize sensor positioning for a damage location problem. The proposed methodology is model-based (FE) and the damage is simulated by elemental removal at the centre of one of each eighteen cells. The aim of this work is to reduce, consecutively, the number of sensors maintaining the levels of successful damage localization. Sensors are, initially, localized around the perimeter of the plate (in a total number of 24 monitored nodes) and transmissibility paths are considered between them. Problem is formulated based on outlier analysis and the transmissibility path(s) chosen will be the one(s) that are more different from the baseline counterpart measurements. Genetic algorithms were used to optimize the search, avoiding the use of combinatorial procedures.

Sensor positioning methodologies are, normally, driven to increase the accuracy of modal identification (such as mode shapes, natural frequencies, etc…). SHM driven sensor positioning methodologies, by other hand, optimize sensor locations to increase sensitivity to induced structural damage. These two different approaches can lead to similar results, in the way that a good modal identification can increase the probability of detecting variations of structural state. However, this is not a rule and SHM dedicated sensor positioning procedures are preferable when the major concern is structural damage detection.

This work describes the first approach followed by Critical Materials S.A. in the context of sensor positioning methodologies using Eigenmode data (retrieved from FE-Finite Element analysis) as the basis information for selecting the most suitable positions for positioning either accelerometers or strain-sensors. It should be noticed that the proposed method is not able to quantify the optimal number of sensors leaving this judgment to the user that, based on the spatial distribution of the proposed sensor positioning metrics, can choose the most suitable zones to install sensors.

Three case-studies (Z-Plate, UAV wing and window panel) are considered for the evaluation of the proposed sensor positioning methodology (see Section 3). Also, experimental verification is conducted, at Critical Materials lab's, for the Z-Plate structure as outlined in Section 5.

2. Sensor Positioning Methodology

The rationale behind the proposed sensor positioning methodology is to avoid positioning sensors in zones of null modal displacement (or stationary vibration nodes). In fact, positioning sensors (such as accelerometers) in zones near vibration nodes (for the defined frequency range) can result in the non-detection of some Eigenmodes and, also, missing important structural resonance peaks. Also, and if strain monitoring is of concern, the proposed method is able to indicate zones in the structure with maximum amplitudes of strain, for the considered analysis frequency range, through compilation of elemental strain energy density obtained for each structural vibration mode.

Finite element data, namely, the data obtained through frequency extraction analysis procedures give us valuable information related with the mode shapes and modal displacement. In fact, the proposed method collects modal displacement information, for the considered frequency range, weights it to the modal effective mass and outputs a normalized scalar metric ranging from 0 to 1, where the maximum value indicate the most suitable positions to install sensors. The method is able to indicate the best spots to positioning accelerometers (or other kinematic-based sensors) based on the collection of nodal displacement. Also, it is possible to positioning strain-gauges (or other types of strain sensors) through the monitoring of elemental output variables such as strain energy (density and total) output variables available in the Abaqus FE code.

Two sensor positioning criteria are defined. If accelerometers are to be positioned in the structure the WMDCr- Weighted Modal Displacement Criteria should be used. In Equation 1, is displayed its expression, where *u* is the modal displacement, *j* the mode number, *i* the node number, and *f* the modal effective mass. For positioning strain sensors is used a criteria based on elemental strain energy, namely, the WMSECr-Weighted Modal Strain Energy Criteria. In Equation 2 is displayed the expression for WMSECr where *k* is the element number and S_{ENER} corresponds to elemental strain energy values. For this case, either strain energy density or total strain energy in the element can be used.

$$WMDCr_i = \frac{\sum_{j=1}^{M} u_i^2 f_j}{\sum_{j=1}^{M} f_j} \qquad (1)$$

$$WMSECr_k = \frac{\sum_{j=1}^{M} S_{ENER_k} f_j}{\sum_{j=1}^{M} f_j} \qquad (2)$$

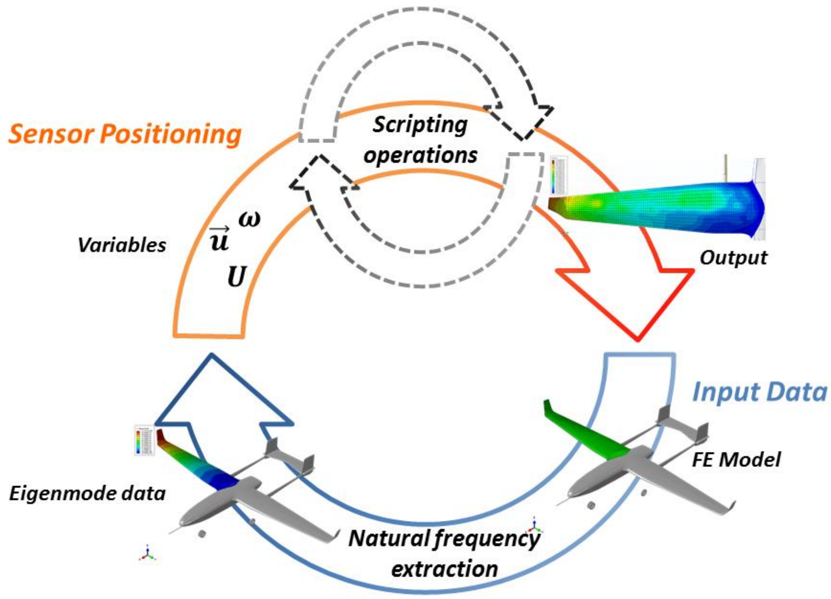

Figure 1 – Conceptual workflow for sensor positioning.

The proposed methodology demands an intensive use of the dynamic analysis procedures made available by Abaqus, namely, Natural Frequency extraction procedures. Also, and in order to systematically collect ant treat relevant output dynamic data, Abaqus scripting capabilities are indispensable to the success of the implementation. In Figure 1, is displayed the conceptual workflow used for sensor positioning procedures and the steps needed to obtain the output of the proposed methodology.

3. Case-Studies

In this section are presented the three models used as case-studies for testing the proposed sensor positioning methodology. In the following sections the model characteristics are detailed.

3.1 Z-Plate

This structure represent a typical aeronautical component whose anti-symmetrical rib reinforcement originate a non-conventional dynamical behavior. The structure is composed by a CFRP laminate (with 5mm thickness) in an epoxy matrix. As visible, in Figure 2, the Z-Plate is fixed, along an entire edge, to a heavy table (200kg) which submits the plate to a cantilever loading condition.

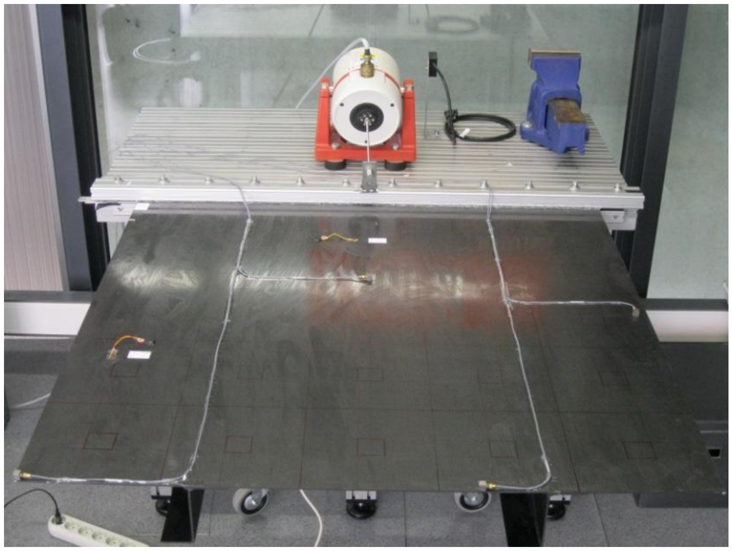

Figure 2 – Z-Plate structure (Experimental setup).

3.1.1 FE model

In Figure 3 is displayed the FE model of the Z-Plate. The model is discretized using 494 quadratic shell elements (S8R). A static gravity step (gravity loading) precedes the natural frequency extraction procedure that was defined for the [0, 1000]Hz frequency range. Lanczos method was considered for the eigenvalue extraction procedure.

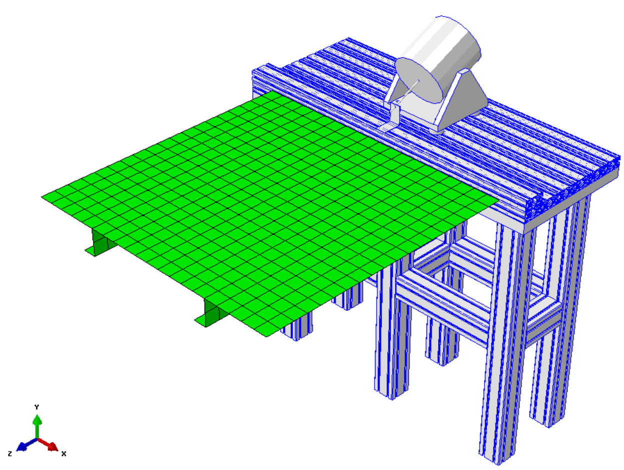

Figure 3 – Z-Plate structure (FE model).

3.1.2 Loading and Boundary conditions

Gravity loading was considered, in order to account the body weight of the structure and stress stiffening effects in the natural frequency extraction procedures. An encastre boundary condition, defined along the fixation edge, is defined in order to simulate the real fixation conditions of the Z-Plate to the experimental table.

3.1.3 Material properties

CFRP's mechanical behavior was considered to be orthotropic. Material properties used in the definition of material properties are summarized in Table 1.

Table 1 Material Properties (CFRP).

E_{11}	$E_{22}=E_{33}$	υ_{12}	G_{12}	G_{13}	G_{23}
42 GPa	42 GPa	0.126	4.5 GPa	4.5 GPa	4.5 GPa

3.2 Window Panel

This structure intends to represents a partial section of an aeronautical fuselage and, for demonstration purposes, it is considered to be supported by an external support as visible in Figure 4.

Figure 4 – Window panel (experimental setup).

3.2.1 FE model

The window panel was discretized using 6516 shell linear elements (S3R and S4R). In order to simplify the fixation structure, only the curved steel frames were modeled and tied to the structure through mesh tie constraints. The other fixation components, belonging to the support structure, were geometrically simplified and defined through connector elements The FE model of the window panel is showed in Figure 5. In order to account the window panel self-weight, a static analysis step was considered. This step precedes the natural frequency extraction procedure that was defined for the [0,500]Hz frequency range.

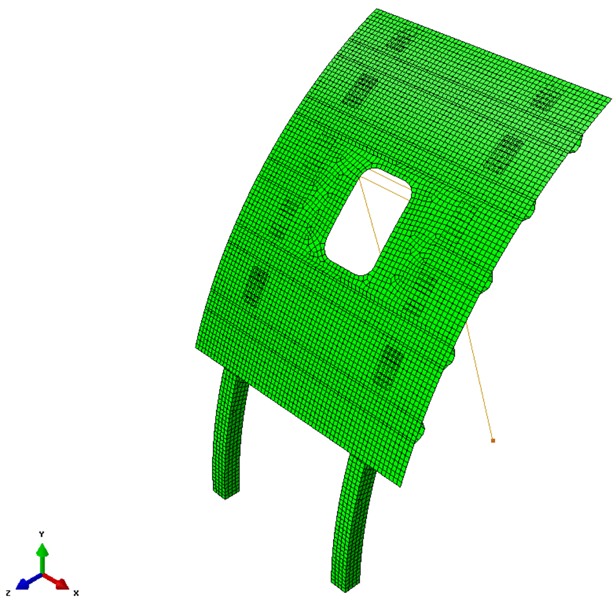

Figure 5 – Window panel structure (FE model).

3.2.2 Loading and Boundary conditions

Body weight loading was introduced in order to account stress-stiffening effects for the subsequent frequency extraction procedures. Boundary conditions were applied directly in the connector elements in order to simulate the fixation of the support structure to the ground.

3.2.3 Material properties

The window panel was produced by vacuum infusion of CFRP-Carbon Fiber Reinforced Polymer and the material was considered to be orthotropic. Material properties used for the constitutive modeling operations are summarized in Table 1.

3.3 UAV wing

A wing of an UAV-Unmanned Armed Vehicle was selected as other example for the application of the proposed sensor positioning methodology. The structure of the UAV is entirely composed by a composite laminate of CFRP in a thermoset epoxy matrix.

3.3.1 FE model

In Figure 6, is showed the FE model of the UAV, considering the mesh discretization of the wing only because the rest of the UAV is defined as a display body. The wing was discretized through 3046 quadratic and linear shell elements (S8R and STRI65).

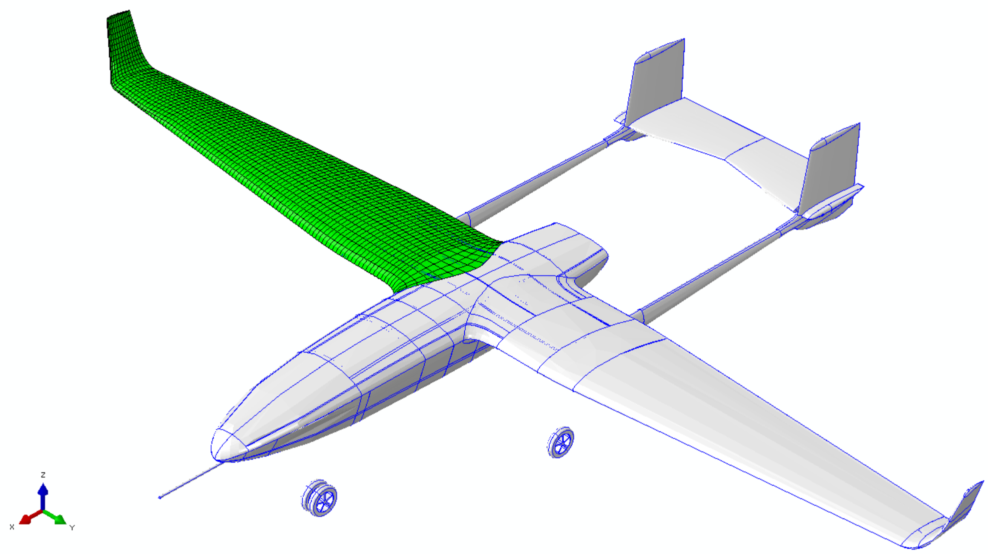

Figure 6 – UAV FE model.

3.3.2 Loading and Boundary conditions

The fixation conditions of wing to the main structure of the UAV were simplified and assumed that the wing's fixation edge is completely stationary. In fact, the wing was considered to be in cantilever state. Gravity loading was introduced in the analysis workflow and a [0, 1000]Hz frequency range was considered for the natural frequency extraction step.

3.3.3 Material properties

In order to maintain consistency with previous constitutive modeling approach, CFRP mechanical behavior was considered to be orthotropic. Material properties used in the definition of material properties are, also, summarized in Table 1.

4. Results

In this section are presented the results, in terms of sensor positioning, obtained for the three considered case-studies

4.1 Z-Plate

In Figure 7, are displayed the first four vibration modes of the Z-Plate corresponding to Eigenfrequencies of 12.37, 13.16, 19.20, and 41.03 Hz, respectively

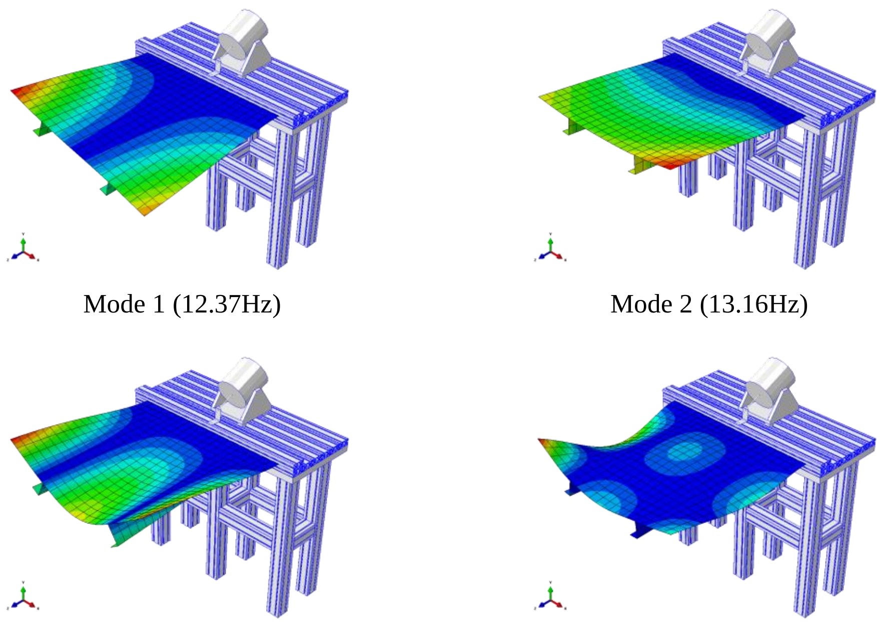

Mode 1 (12.37Hz) Mode 2 (13.16Hz)

Mode 3 (19.20Hz) Mode 4 (41.03Hz)

Figure 7 – First four vibration modes (Z-Plate).

In Figure 8, for a frequency range of [0, 1000]Hz, is displayed the WMDCr field output for the Z-Plate. Also, in Figure 9, and for the same frequency range, is displayed the WMSECr field output.

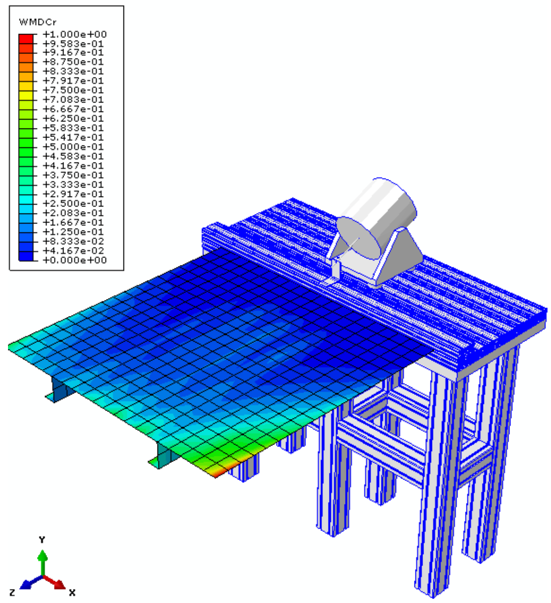

Figure 8 – WMDCr field for accelerometer positioning (Z-Plate).

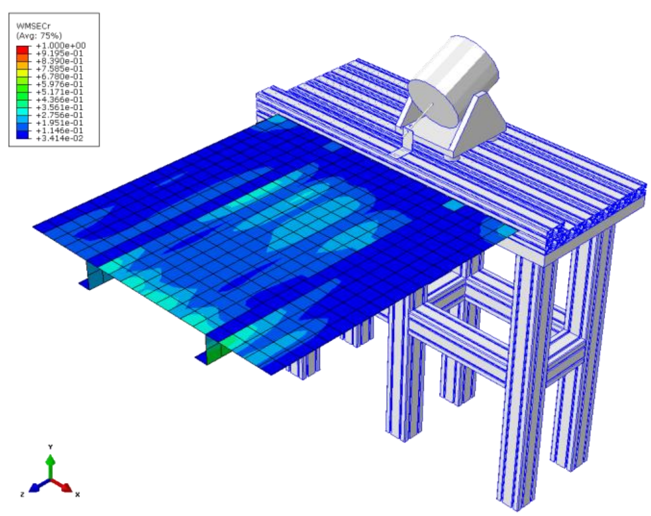

Figure 9 – WMSECr field for strain-sensor positioning (Z-Plate).

4.2 Window Panel

In Figure 10, are displayed the first four vibration modes of the window panel corresponding, respectively, to 31.80, 32.92, 72.59, and 101.43 Hz natural frequency values.

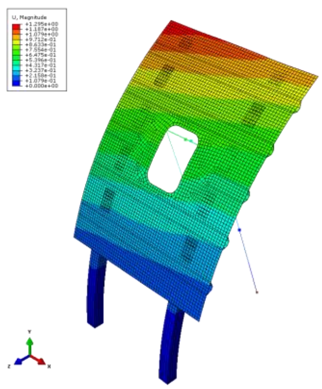

Mode 1 (31.80Hz)

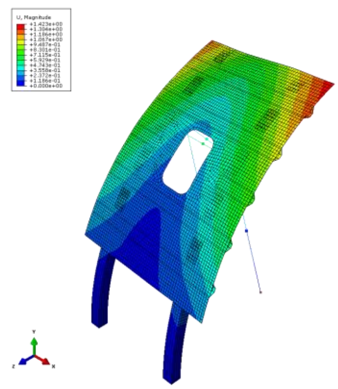

Mode 2 (32.92Hz)

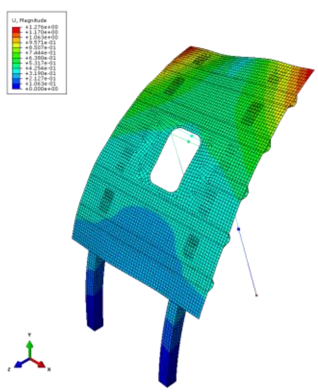

Mode 3 (72.59Hz)

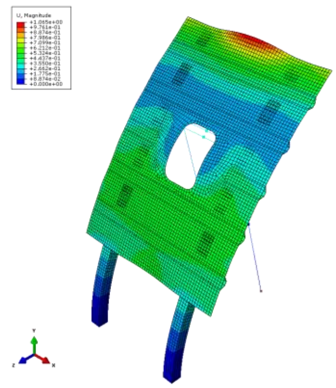

Mode 4 (101.43Hz)

Figure 10 – First four vibration modes (window panel).

In Figure 11, is displayed the WMDCr field output, for the window panel, considering as evaluation criteria the normal to the surface modal displacement. In Figure 12, is displayed the strain related WMSECr field output.

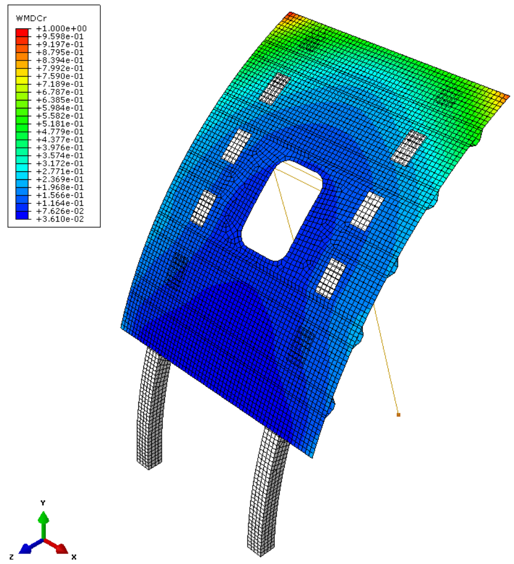

Figure 11 – WMDCr field for accelerometer positioning (window panel).

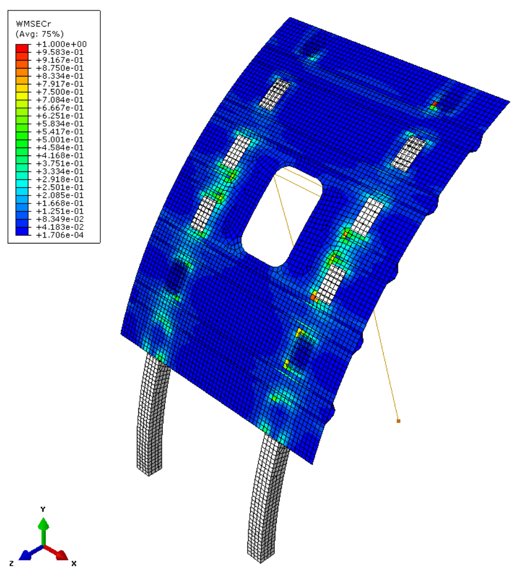

Figure 12 – WMSECr field for strain-sensor positioning (window panel).

4.3 UAV wing

In Figure 13 is displayed the first four vibration modes of the Z-Plate corresponding to 11.41, 42.13, 54.83, and 65.27Hz, respectively

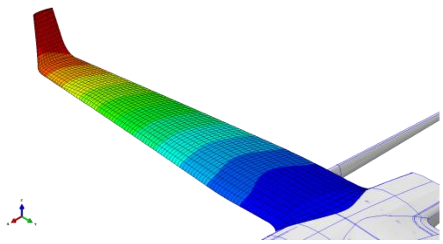

Mode 1 (11.41Hz)

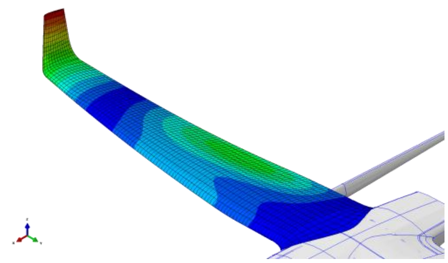

Mode 2 (42.13Hz)

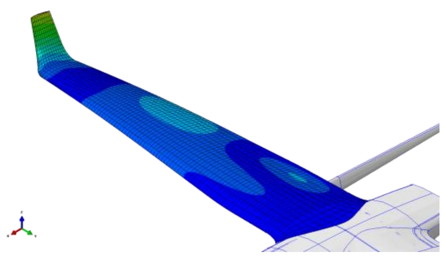

Mode 3 (54.83Hz)

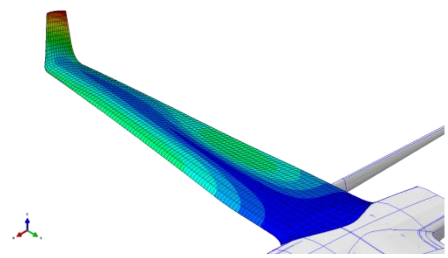

Mode 4 (65.27Hz)

Figure 13 – First four vibration modes (UAV wing).

In Figure 14, and for a frequency range of [0, 1000]Hz, is displayed the WMDCr for the UAV wing while, in Figure 15, is displayed the WMSECr field output.

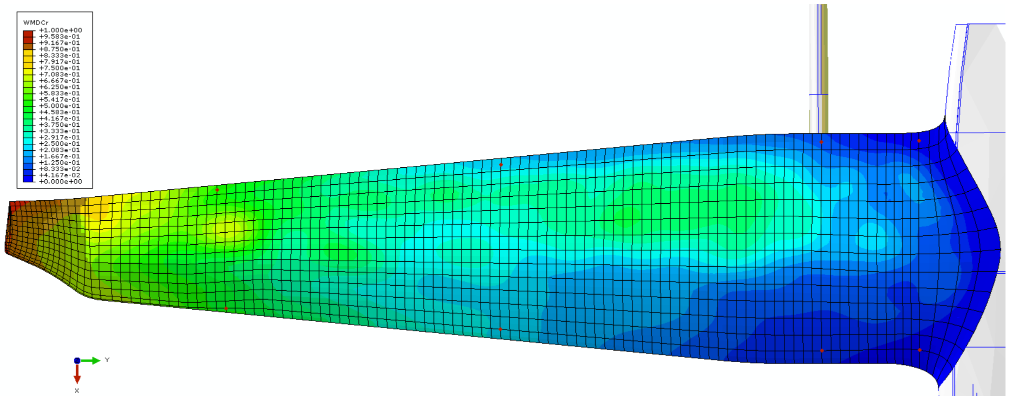

Figure 14 – WMDCr field for accelerometer positioning (UAV wing).

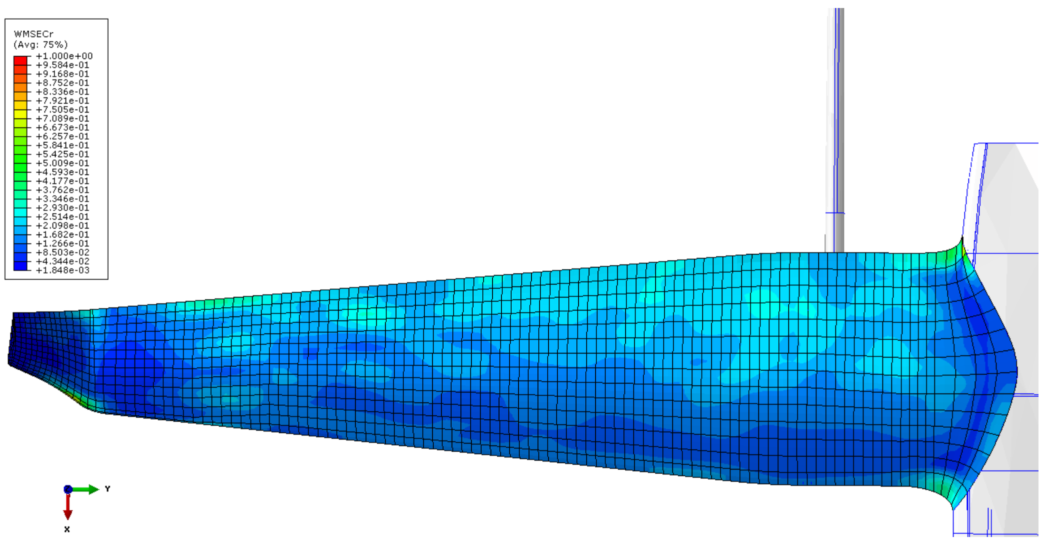

Figure 15 – WMSECr field for strain-sensor positioning (UAV wing).

5. Experimental Evaluation

The accuracy of the proposed sensor positioning method was evaluated for accelerometer positioning (based on the WMDCr) considering the Z-Plate structure displayed in Figure 2. The mobility transfer function was outputted for each evaluated point and the number of resonance peaks, that obeys the 3dB bandwidth method, counted and compared.

5.1 Experimental setup

In Figure 16, are displayed the points chosen for the experimental tests considering maximum and minimum values for the considered sensor positioning criteria (WMDCr). Six points were chosen, as the basis points for testing the accuracy of the methodology. Following the transfer function reciprocity method, a uniaxial accelerometer was attached to the point with maximum value of WMDRc (point relative to sensor A) and the transfer functions were outputted impacting, with an instrumented hammer, all the selected points as displayed in Figure 17 and Figure 18.

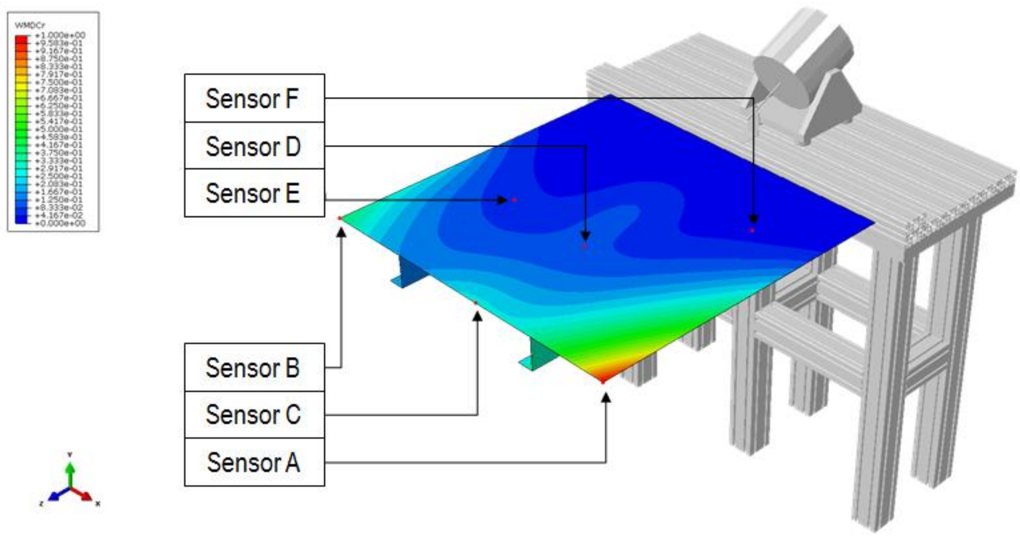

Figure 16 – Selected points for accelerometer positioning.

In Table 2 is established the correspondence between the selected points and respective WMDCr values.

Table 2 Selected sensor locations and associated WMDCr.

Sensor	WMDCr
A	1.0
B	0.403681
C	0.293081
D	0.099282
E	0.058529
F	0.025289

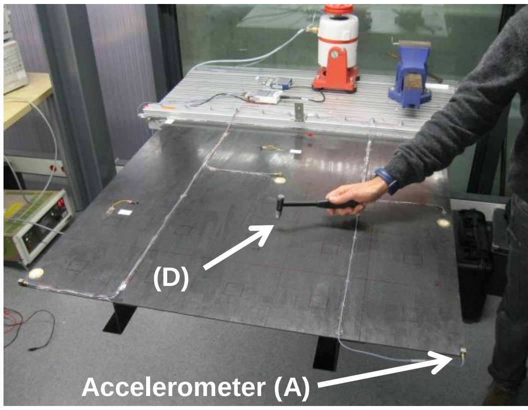

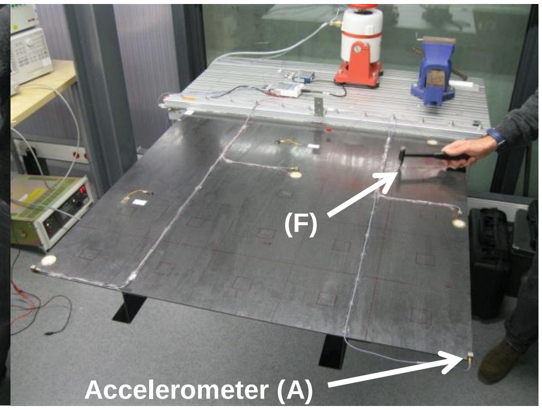

Figure 17 – Impacting point D. **Figure 18 – Impacting point F.**

5.2 Experimental results

To test the effectiveness of the sensor positioning method, the mobility transfer function spectrum was computed for each sensor position and the number of resonance peaks, that obey the 3dB bandwidth method, counted. This approach intends to reveal the quality of the dynamic signal that is related with the number of modes extracted from the monitored point.

In Figure 19, and as an example, is displayed the mobility transfer function spectrum for sensor location B, considering a [0,200]Hz frequency range.

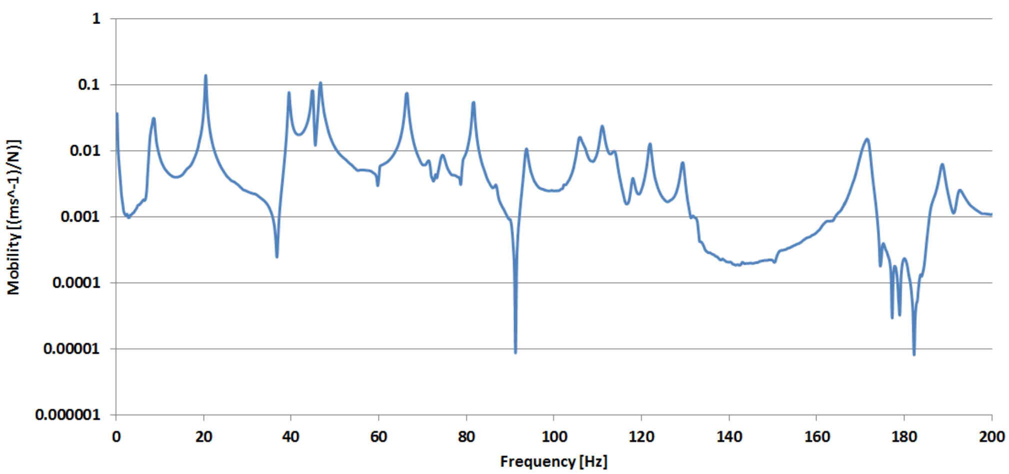

Figure 19 – Mobility frequency response function (sensor location B).

The relationship between the number of resonance peaks and the sensor positioning criteria

(WMDCr), obtained for the six selected points (see Table 2), is displayed in Figure 20.

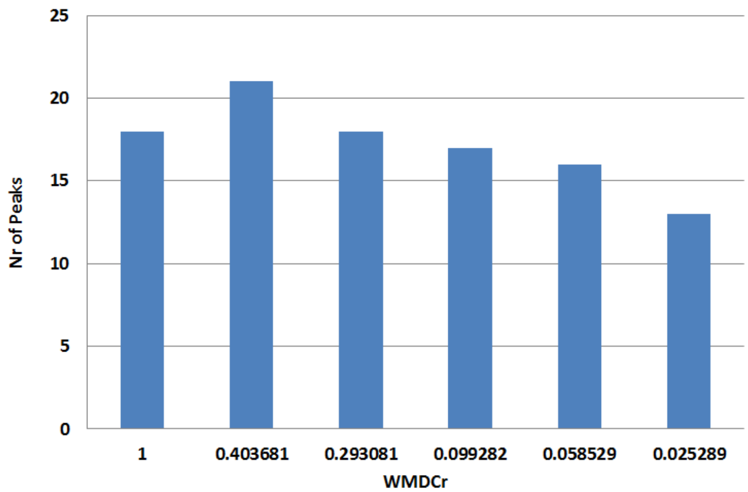

Figure 20 – Evolution of number of peaks with WMDCr for [0,200]Hz.

6. Results Discussion

From the observation of WMDCr it is possible to conclude that zones away from fixation boundary conditions are more suitable to positioning sensors such as accelerometers. In fact, from the observation of results displayed in Figure 8 and Figure 14, the criterion (WMDCr) is maximum on those zones. The boundary and loading conditions, of both these models, implies a continuous displacement for all the nodes in those zones for the considered frequency range, while zones located near the boundary conditions can be affected by stationary vibration nodes. For the window panel case it is visible that zone located at the top of the structure are more suitable to receive accelerometers, as displayed in Figure 11.

In contrast, for strain sensors positioning is more difficult to establish a standard in terms of strain sensor positioning. In fact, and as displayed in Figure 9 and Figure 15, where WMSECr field output is plotted, zones adjacent and apart from the boundary conditions are suitable to receive strain sensors. The geometrical configuration of the mode shapes, the associated differential displacement and the considered frequency range could contribute to this behaviour.

In Figure 12, is displayed the strain positioning field for the window panel. It is clear, from the observation of the field output, that strain sensors should be positioned near the fixation frames. In fact, strain amplitudes can be maximum, in these zones, due to a localized constrained displacement and consequent increase of the differential of displacement.

The conducted experimental tests reveal that the number of valid resonance peaks decrease with the WMDCr. In fact, and observing the graph in Figure 20, the number of peaks is minimum for sensor location F and maximum for sensor location B followed by point A. However, it should be noticed that, following this understanding, the number of resonance peaks should be maximum for the sensor location A. In fact, for this point the obtained result is not coherent, with the trend obtained for the other tested points. This behavior may be related to the impossibility of impacting it correctly due to the fixation of the accelerometer in this point and the need of offsetting the impact point from the installed accelerometer.

To try to overcome this inconsistency, a different evaluation metric can be tested and the results compared with the already implemented one. One of the possible metrics that could be used is the comparison of the modal damping for a set of modes available in all the considered test points.

7. Conclusions

The proposed method showed potentialities in terms of sensor positioning that can have a huge interest for application in modal analysis procedures. In fact, and after conducting experimental tests, it was showed that the WMDCr can be related with the quality of experimental dynamic signal obtained, which, for this work, was quantified through the number of obtained resonance peaks obeying to the 3dB bandwidth method. However, some questions are still open. The incoherency of results associated to some sensor locations, namely sensor location A, and the dependency of sensor positioning accuracy with the analysis frequency range, should be carefully studied in future works.

8. Bibliography

BASSEVILLE, M., BENVENISTE, A., MOUSTAKIDES, G. V. & ROUGEE, A., 1987. Optimal Sensor Location for Detecting Changes in Dynamical Behavior. *IEEE TRANSACTIONS ON AUTOMATIC CONTROL,* Volume 12, pp. 1067-1075.

Beal, J. M., Shukla, A., Brezhneva, O. A. & Abramson, M. A., 2008. Optimal sensor placement for enhancing sensitivity to change in stiffness for structural health monitoring. *Optimization and Engineering,* Volume 9(2), pp. 119-142.

Hanis, T. & Hromick, M., 2012. Optimal sensors placement and spillover supression. *Mechanical Systems and Signal Processing,* Volume 28, pp. 367-378.

Lia, D., Lia, H. & Fritzen, C., 2007. The connection between effective independence and modal kinetic energy methods for sensor placement. *Journal of Sound and Vibration,* Volume Volume 305, p. 945–955.

Manson, G. & Worden, K., 2001. *Sensor optimisation for a damage location problem.* s.l., s.n.

Meo, M. & Zumpano, G., 2005. On the optimal sensor placement techniques for a bridge structure. *Engineering Structures,* Volume 27, p. 1488–1497.

Staszewski, W. J. & Worden, K., 2001. *An Overview of Optimal Sensor Location Methods for Damage Detection.* s.l., s.n., pp. 179-187.

Worden, K. & Burrows, A., 2001 . Optimal sensor placement for fault detection. *Engineering Structures,* Volume 23, p. 885–901.